Electronic Supplementary Information (ESI)

Efficient infrared sunlight absorbers based on gold-covered, inverted silicon pyramid arrays

Jinhui Hu[a], Luis A. Pérez[a,*], Juan Luis Garcia-Pomar[b], Agustín Mihi[a], Miquel Garriga[a], M. Isabel Alonso[a], Alejandro R. Goñi[a,c,**]

[*]lperez@icmab.es, [**]goni@icmab.es

[a]*Institut de Ciència de Materials de Barcelona, ICMAB-CSIC, Campus UAB, 08193 Bellaterra, Spain*

[b]*INL-International Iberian Nanotechnology Laboratory, Av. Mestre José Veiga s/n, 4715-330 Braga, Portugal*

[c]*ICREA, Passeig Lluís Companys 23, 08010 Barcelona, Spain*

Fabrication of inverted micro-pyramids:

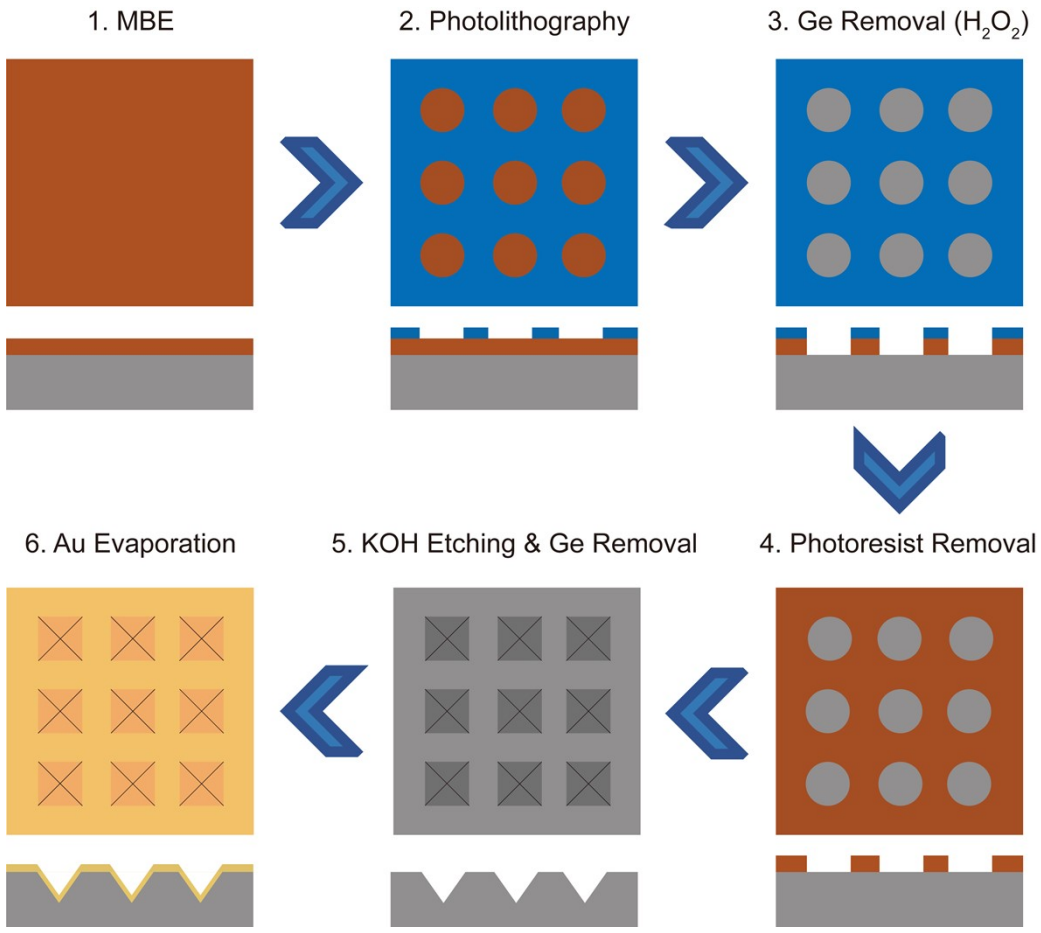

Figure S1: Different steps of the fabrication procedure of microns-size inverted pyramids by conventional photolithography and wet KOH etching.

A sketch of the different steps of the fabrication procedure by conventional photolithography and wet KOH etching is displayed in Fig. S1. For the fabrication of microns-size pyramids a 1200 nm-thick Shipley resist was deposited on Si/Ge heterostructure. Then, a pattern of holes with the desired diameter and pitch is printed on the resist with a microwriter under exposition with a UV laser, subsequently developed and rinsed with water. A wet H_2O_2 etching was carried out to remove rest of the Ge in the holes. An anisotropic wet etching in 33wt% KOH produced the inverted pyramids in the exposed Si. Finally, a 50 nm thick Au film was deposited by thermal evaporation on the surface of inverted pyramid.

Numerical Simulation:

As shown in Fig. S2, the unit cell of the inverted pyramid structure was set as the simulation region using periodic boundary conditions (PBC) along the x and y axes and perfectly matched layer conditions along the z-axis. The pyramid and the surrounding medium were divided into a mesh (not shown) for computing the finite differences.

A script written to separate the zeroth order from the calculated total optical response of the pyramid arrays is freely available at the data repository Zenodo: https://doi.org/10.5281/zenodo.5669255

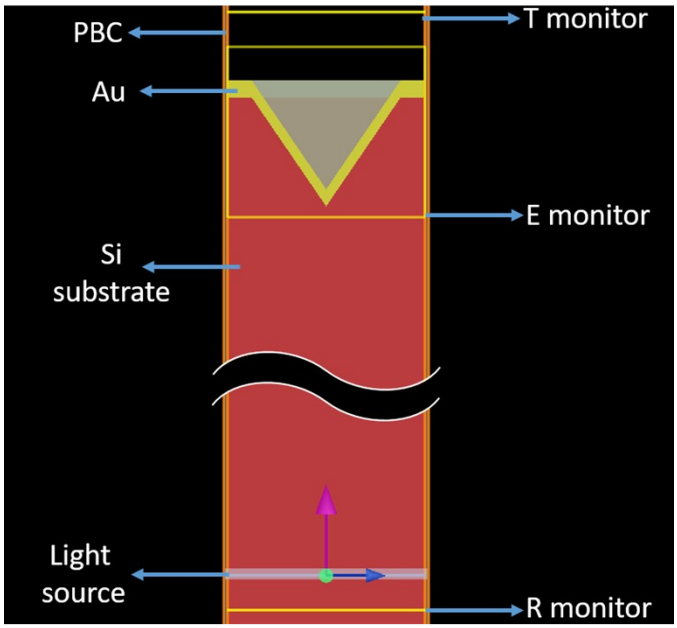

Figure S2: FDTD simulation model of the inverted-pyramid unit cell with periodic boundary conditions (PBC). Different elements are indicated by arrows like the light source, the Si substrate, the gold layer as well as the reflection (R), transmission (T) and electric-field (E) monitors.

Pre-screening of pyramid array parameters:

In Fig. S3, we show the pre-screening of the gold layer thickness. The result is straightforward: With increasing Au thickness light absorption increases rapidly from zero to a saturation value, reached above a thickness of ca. 30 nm. Consequently, we deposited routinely 50 nm of gold, so as to obtain smooth, strongly-absorbing Au layers.

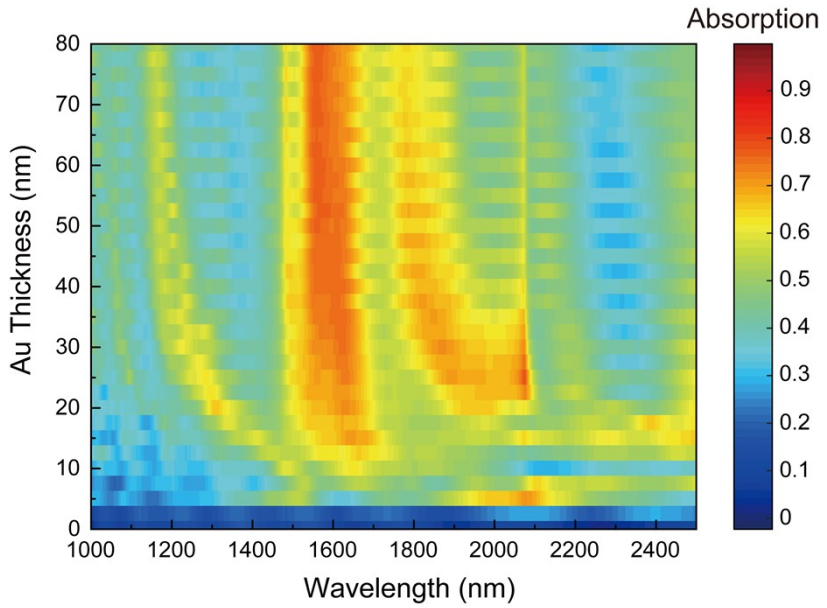

Figure S3: Contour plots of the normalized absorption as a function of the Au film thickness for a structure with L= 500 nm, LP= 600 nm.

Internal photoemission of hot-electron & hot spots:

Figure S4 depicts a simplified scheme of an internal photoemission device based on inverted pyramids and the corresponding electron potential profile along a cross section through the centre of the pyramid (dashed line in Fig. 4a). The pyramids were engraved onto a sufficiently thick and undoped Si layer, previously deposited on top of a n-doped Si substrate. A Schottky barrier forms at the metal-semiconductor interface due to band bending effects in the semiconductor. This occurs because of the pinning of the Fermi level at midgap by surface states in undoped silicon, whereas in n-type Si the Fermi level lies close to the bottom of the conduction band. The doping level of the substrate was selected such that it has simultaneously a low electrical resistivity and negligible free-carrier absorption for light in the NIR spectral range. As illustrated, NIR photons with energy □ω, coming from the substrate side, resonantly

excite a particular plasmon mode, characterized by having hot spots in its near field. These hot spots are the ones that lead to the emission of a hot electron across the barrier upon relaxation of the photoexcited plasmon. Hot electrons are expected to be ejected mainly from hot spots, because the electric field at the metal/semiconductor interface is highly enhanced with respect to the incident field and exhibit large vector components perpendicular to the interface.

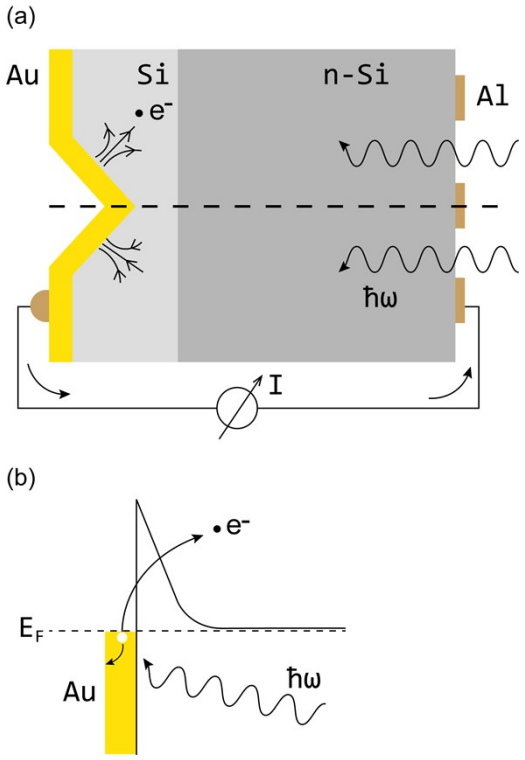

Figure S4: (a) Sketch of a possible hot-electron internal-photoemission Au/Si/n-Si/Al device based on inverted pyramids. **(b)** Profile of the electron potential along the dashed line in (a).

Calculated near-field properties:

For S-polarized light (perpendicular to the plane of the monitors) the electromagnetic field is concentrated in regions close to the pyramid facets and tip but clearly separated from the Au/Si interfaces, as depicted in Fig. S5. This is evidence of an outspoken photonic character of the S-polarized component of both resonant modes. In this case, the maximum intensity enhancement remains always below one order of magnitude.

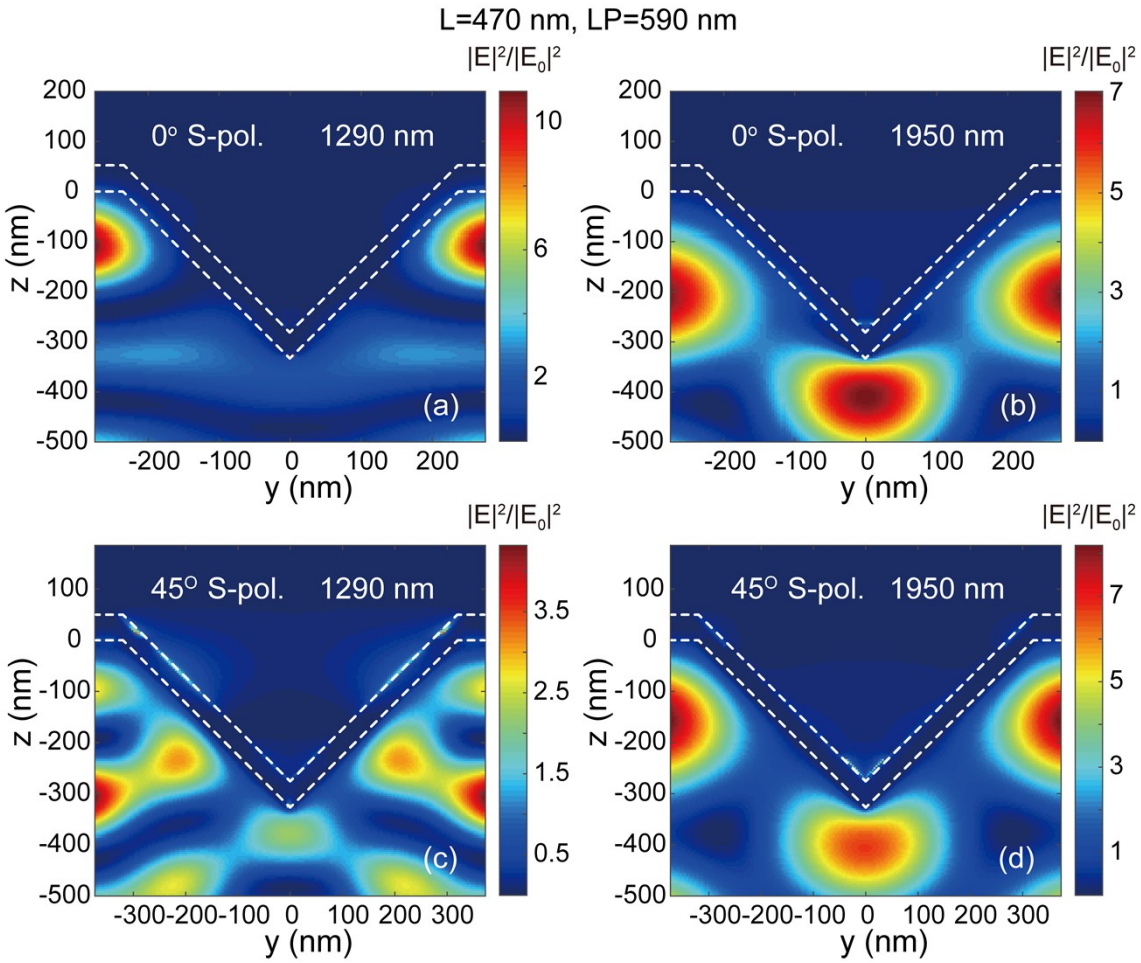

Figure S5: Near-field properties of small inverted pyramids (L=470 nm, LP= 590 nm) covered with 50 nm of Au. The light is in all cases S-polarized, i.e. perpendicular to the monitor plane. **(a),(b)** Case of 0º monitor, S-polarized light of 1290 nm and 1950 nm, respectively. **(c),(d) C**ase of 45º monitor, S-polarized light of 1290 nm and 1950 nm, respectively.

In contrast to the S-polarized components, the near fields associated with the P-polarized components produce large concentrations of charges at points or localized regions right on the surface of the inverted pyramids, the so-called hot spots, for which the electric-field vectors are perpendicular to the metal surface at the hot spots. This can be visualized in Fig. S6, where we overlay the electric-field vectors to the intensity contour plots of Fig. 7 of the manuscript for the 0º monitor. An inspection of the field lines obtained from the FDTD calculations reveals that the hot spots on each facet correspond to the end-point charges of a sort of electrical dipole, oscillating with the same frequency of the incident light. Furthermore, the two dipoles in confronted facets are by symmetry in exact opposition. The effective net charge at each end of the dipoles or the charge separation might vary for different modes (wavelengths) and different

monitors but for pyramid of this size we always find that NIR light induces two dipoles in opposition on the pyramid facets.

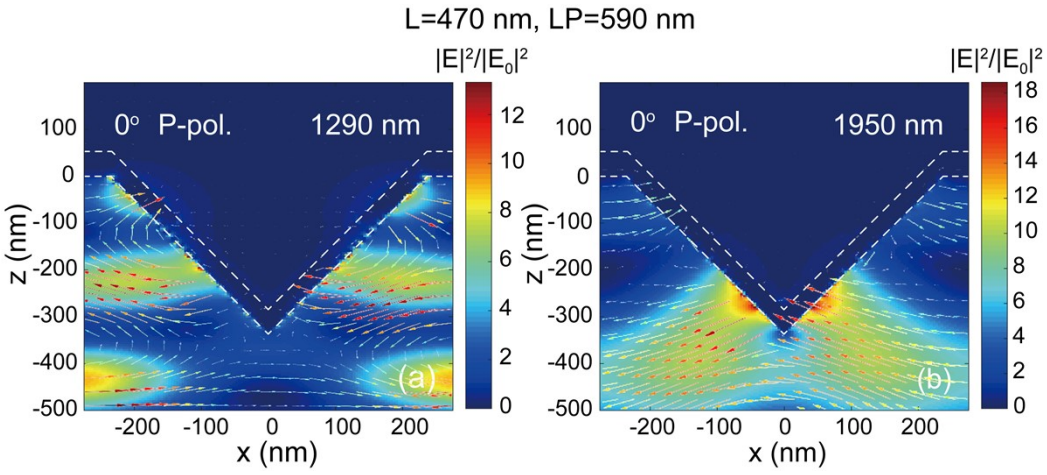

Figure S6: Visualization of the electric-field vectors for the near-field distributions calculated for P-polarized light, 0º monitor, at **(a)** 1290 nm and **(b)** 1950 nm for a small Au-covered, inverted pyramid array (L=470 nm, LP= 590 nm), corresponding to Figs. 9b and 9c.

For large, microns-size pyramids their potential for hot-electron generation is less encouraging. Figure S7 displays the contour plots of the electric-field intensity of an array of large pyramids (L=4.1 μm, LP=6.0 μm) at two resonant wavelengths of 1450 and 1760 nm for both P and S-polarized NIR light with respect to a 0º monitor. The field-intensity distribution reveals that these modes possess mainly photonic character, i.e. they are Bragg-like modes. Except for a few moderately intense hot spots for P-polarization at 1450 nm, all other field enhancements occur away from the metal surface in the space between the pyramids inside the silicon. The hot spots, however, now correspond to the end points of a series of dipoles aligned in head-to-tail manner along the pyramid facets.

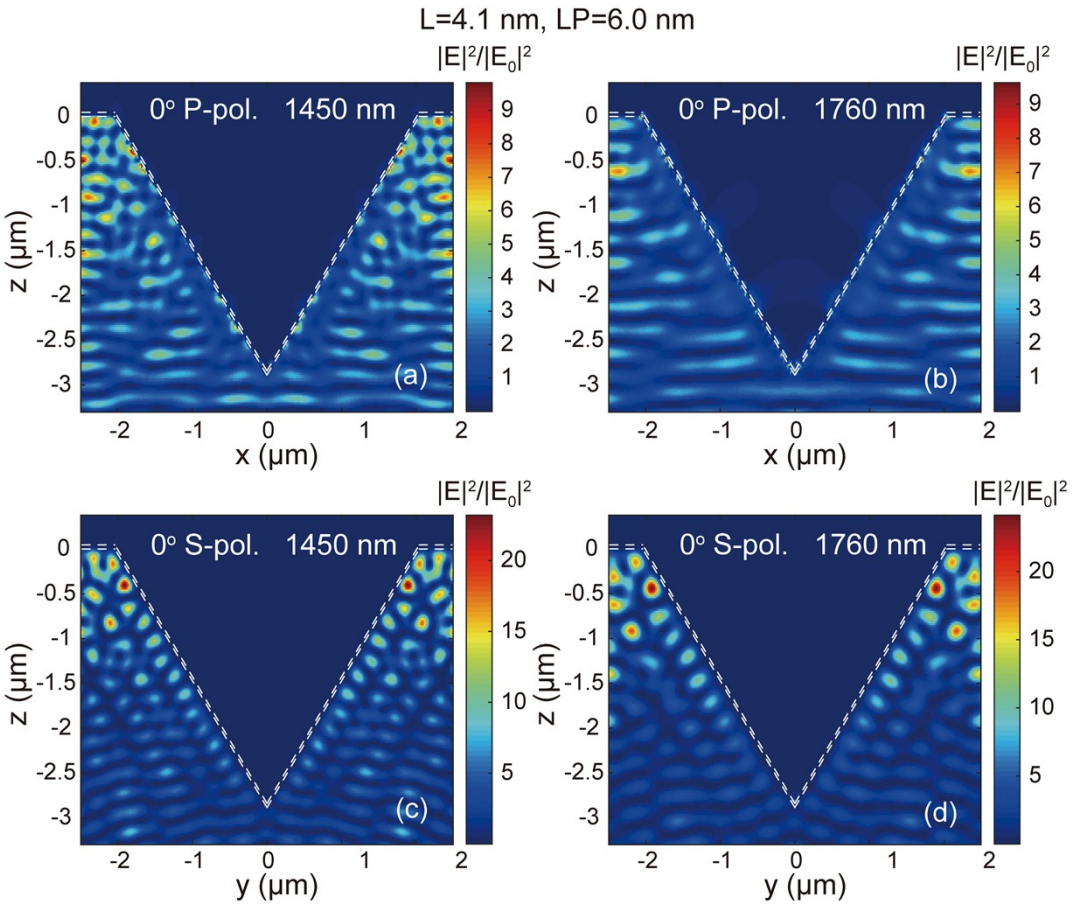

Figure S7: Near-field distribution of the electric-field intensity across 0º monitors for **(a), (b)** P-polarized light of 1450 nm and 1760 nm, respectively, and **(c), (d)** for S-polarized light of 1450 nm and 1760 nm, respectively, in the case of an array of gold-covered, large inverted pyramids (L=4.1 μm, LP= 6.0 μm).